Molecular Architectonics, The Third Stage of Single Molecule Electronics, Ed. T. Ogawa, Springer, pp.355-379 (2017)

Electron transport through a single molecule in scanning tunneling microscopy junction

N. Takagi[1] and R. Hiraoka[1,$]

[1]Department of Advanced Materials Science, The University of Tokyo, 5-1-5 Kashiwanoha, Kashiwa, Chiba 277-8651 Japan

[$]present address: Tsukuba Material Development Laboratory, Sumitomo Chemical Co., Ltd., 6 Kitahara, Tsukuba, Ibaraki 300-3294, Japan

Abstract

A single molecule junction (SMJ), a molecule bridging two metal electrodes, is a primitive model of molecular electronic devices and provides a unique platform to resolve fundamental questions how the electrical current flows through a single molecule and what functionality emerges arising from the original characteristics of the molecule. Recently, the conductance values of various molecules have been measured experimentally by using mechanically controllable break junction (MCBJ) and scanning tunneling microscopy (STM) junction. The accumulated database combined with first-principles theoretical calculations enables us to discuss the relation of the transport characteristics with the geometrical configuration of molecule in the junction, the molecule electronic structure, and the molecule-electrode coupling. Although the conductance is always analyzed by using Landauer formula, it is still challenging to experimentally partition the conductance to the contributions from multiple transport channels and determine the total number of transport channels and their transmission probabilities. These quantities provide deeper insights on the electron transport through a single molecule and specify the SMJ like a personal identification number (PIN) code. This chapter describes a method to determine the “PIN” code based on multiple Andreev reflections (MARs) and demonstrates the application to a C_{60}-SMJ fabricated with STM technique.

1. Background

Since the discovery of transistor [1], electronic devices based on solid state semiconductors have been remarkably evolved. Advance in semiconductor technology has realized high-performance chips in which numerous tiny transistors are densely integrated. These chips are used inside various types of electronic equipment such as personal computer, mobile phone, household electric appliances and etc., and provide solid foundation to our highly-networked information society. Although typical chips invented in the 1960's contained only several transistors, the number of transistors in a chip has increased dramatically year by year as usually stated by Moor's law [2]. The chips at the heart of a present mobile phone are constructed from more than a few billions of transistors whose sizes are sub-100 nanometers on average. The density of transistors will furthermore increase several years later. According to the International Technology Roadmap for Semiconductors 2013, the target of half pitch size of logic gate is 7 nm in 2028 [3]. The accelerated miniaturization and high integration of electronic circuits are reaching certain limitations, however. The circuits based on the solid state semiconductors cannot be downsized to a nanometer scale from the fundamental physics law that the wave-particle dual nature of electron emerges and violates the fundamental principles of the transistor operation. In addition, the fabrication cost skyrockets so that an individual company hardly returns on the huge investment. Solutions to overcome these problems and alternative strategies to fabricate next-generation electronic devices are intensively required.

One of the solutions is use of organic molecule as a building block in the heart of the electronic device. As a result, single molecule device has attracted considerable attentions. Single molecule device is a device that a single molecule plays a key role in the functionality. Compared to the solid state semiconductors, the expected advantages of the single molecule device are as follows: (i) a molecule is so small as a nanometer scale, flexible and stable compared to nanostructures consisting of metals and semiconductors, and (ii) the various classes of molecules can be designed and synthesized, leading to unique functionalities which are difficult to be realized by bulk materials. In addition to these points, the use of magnetic molecules such as a single molecule magnet (SMM) [4] paves a way to realize spin-based electronic device in which both charge and spin degrees of freedom of electron are utilized.

The history of single molecule device goes back to 1974 when Aviram and Ratner (abbreviated as AR) proposed a basic concept [5]. Stimulated by both progress in the semiconductor electronic devices and development of electron-conductive organic materials, AR theoretically considered a single molecule junction (SMJ) in which a molecule connects with two metallic electrodes. The molecule

consists of tetracyanoquinodimethane (TCNQ), tetrathiafulvalene (TTF) and a methylene bridge (see Fig. 1). The methylene bridge electronically decouples the TCNQ and TTF molecules. The constituent TCNQ and TTF molecules are typical acceptor and donor molecules, respectively, and the designed molecule is a mimic of p-n junction. When the couplings with the metallic electrodes are not strong, the entire electronic structure is well described as a sum of those of the isolated molecules. The energy diagram indicates that this SMJ shows a nonlinear I-V characteristic and works as a rectifier. Although the model was simple, their work opened a new research field and stimulated a vast number of studies in the past several decades.

2. Basic theory of electron transport through nanoscale conductors

To begin with, we briefly introduce the carrier transport in the macroscopic conductor. The conductance G (inverse of resistivity) of the macroscopic conductor, the electrical current I through the conductor and applied the bias voltage V obey the Ohm's law. The conductance is described as $G = \frac{I}{V} = \sigma\frac{A}{L}$, where σ is the conductivity and A and L represent the cross sectional area and the length of the conductor, respectively. The conductance depends on the conductivity inherent to the material and the dimensions of the conductor. In a more detail description based on the quantum physics, the electron transport is described by using the Boltzmann equation under the relaxation-time approximation [6]. As an instance, σ of a three-dimensional isotropic simple metal is given by

$$\sigma = \frac{1}{3}e^2\tau_{relax}v_F\rho_F \quad (1)$$

where e is the elementary charge, v_F is the Fermi velocity of electron, τ_{relax} is the relaxation time and ρ_F is the density of states (DOS) at the Fermi energy (E_F). Obviously, σ varies from material to material; v_F and ρ_F reflect the electronic band structure of the conductor.

In contrast, decreasing the scale of the conductor to the mesoscopic regime, the above model based on the electron scattering is no longer valid because the mean free path of electron is comparable to the size of the conductor and electrons can pass through the conductor without being scattered. In other words, the electron can transmit coherently as a wave, without losing the phase memory of its wave function. The electron transport through the mesoscopic conductor was first theoretically considered by Landauer [7-9], who showed that the conductance is quantized to a universal value known as conductance quantum, $G_0 = \frac{2e^2}{h} \approx (12.9\mathrm{k\Omega})^{-1}$, where h is the Planck constant. When there are n channels carrying the electrical current across the junction, the total conductance is expressed as

$$G = G_0 \sum_{i=1}^{n} \tau_i \quad (2)$$

where τ_i is the transmission probability of i-th transport channel. This is called the Landauer formula.

Here, we employ a simple one-dimensional junction and derive the Landauer formula below [10]. The junction consists of a small conductor bridging two electrodes as shown in Fig. 2. We introduce the following assumptions:

- The conductor has a single channel or an electronic state responsible for the electron transport.
- The temperature is absolute zero so that the electronic states under the chemical potential are fully occupied. The electron-electron Coulomb interaction is neglected.
- The bias voltage V applied to the conductor causes a potential difference between the left and right electrodes, $eV = \mu_L - \mu_R$, where μ_L and μ_R are the chemical potentials of two electrodes.
- Each electrode is sufficiently large and has lots of electronic states and thus it can be regarded as an electron reservoir. All the electrons reaching the electrodes are rapidly relaxed so that the electrodes are preserved in the equilibrium even when the current flows.
- There is no scattering and reflection of electron inside the conductor as well as at the interfaces between the conductor and the electrodes. The transmission probability is assumed to be equal to 1.

Under these assumptions, the electrical current carried by the electron with wave number k is expressed as

$$j(k) = \frac{2\pi e}{h} \frac{1}{L} \frac{dE(k)}{dk} \quad (3)$$

where L is the length of the conductor and $E(k)$ represents the energy band structure of the electron. The total current I across the conductor is obtained by summing the currents carried by the electrons which energies are within the range of $eV = \mu_L - \mu_R$:

$$I = 2\int_{k(\mu_R)}^{k(\mu_L)} j(k) \frac{L}{2\pi} dk = \frac{2e}{h} \int_{\mu_R}^{\mu_L} dE = \frac{2e^2}{h} V \quad (4)$$

where we include the spin degrees of freedom of electron. The conductance is obtained:

$$G = \frac{I}{V} = \frac{2e^2}{h} \approx (12.9\mathrm{k\Omega})^{-1}. \quad (5)$$

This equation indicates that the mesoscopic conductor with a single transport channel has a universal conductance of $G_0 = \frac{2e^2}{h}$ which does not depend on the dimensions and the band structure contrasting

to the macroscopic conductor. When there are n channels, the conductance is nG_0. Including the reflection of electrons at the interface, the Landauer formula [eq. (2)] is derived. The formula provides a solid foundation to evaluate the transport characteristics of nanoscale conductors from quantum point contact fabricated with solid state semiconductors, metallic atomic wire to SMJ. Although it is challenging to evaluate the conductance of a single molecule, recent advent of experimental techniques such as mechanically controllable break junction (MCBJ) and scanning tunneling microscopy (STM) enables us to measure the conductance of a single molecule.

3. Experimental techniques to evaluate the conductance of a single molecule

The experimental set-ups of MCBJ and STM are schematically illustrated in Figs. 3 (a) and (b), respectively. In the MCBJ measurement [11, 12], a metal wire with a notch is placed and glued on a stage covered with an insulating film. A piezoelectric device under the stage pushes and bends the stage to break the wire at the notch; as a result, a pair of clean metallic electrodes is formed. The conductance between the electrodes is measured as a function of the distance between the electrodes by bending the stage. Repeating the procedure more than thousands times, a statistical data set is collected as a conductance histogram. When stable atomic-sized contacts are constructed, peaks emerge in the histogram and then conductance values inherent to the contacts are determined. The same procedure is carried out under the atmosphere of a molecule to measure the conductance of the SMJ. When the gap distance matches with the molecular size to accommodate the molecule in between the electrodes, a peak is observed in the conductance histogram. Finally, the conductance of the molecule is determined from the histogram. In addition, when the stable SMJ is fabricated, we can even acquire the vibrational fingerprint of the molecule by measuring the I-V characteristic at cryogenic temperature and identify the molecule configuration with respect to the electrodes [13, 14].

Although MCBJ is powerful, MCBJ does not provide the direct information on the molecule configuration inside the junction because it is not visible by this method. In addition, the conductance measured by MCBJ is a statistical average over the various configurations of molecule and electrodes, and thus important information may be buried by the statistical procedure. STM provides a chance to overcome these problems. We can fabricate SMJ with STM similarly to MCBJ by adjusting the position of an STM tip over a molecule on a metal substrate, approaching the tip to the molecule and touching the molecule with the tip [see Fig. 3 (b)]. Using the tip and the substrate as metallic electrodes, we can measure the I-V characteristic and determine the conductance of the molecule. This method is superior

to MCBJ in the following points: First, we can determine the orientation and adsorption site of the molecule by visualizing the molecule in atomic resolution. Second, we can address the contact position inside the molecule accurately and fabricate the SMJ when the molecule consists of multiple functional groups. This enables us to measure the dependence of conductance on the contact positions. Finally, we can characterize the molecule by acquiring one-electron energy spectrum [15, 16], vibrational spectrum [17, 18] and spin spectrum [19, 20] of the molecule with scanning tunneling spectroscopy (STS) and inelastic electron tunneling spectroscopy (IETS). Actually, contacting the tip with the molecule might modify the molecule configuration and electronic structure when the SMJ is formed. However, the characterization of the molecule before fabricating the SMJ helps us understand the transport characteristics.

The conductances of various kinds of molecules have been investigated mainly by MCBJ and STM [21-42]. The conductances of organic molecules are well described as $G = A\exp(-\lambda L)$ where A is a constant, L is the molecular length, and λ is a constant related to the molecular electronic structure [43]. The molecules exhibiting higher conductances have smaller λ values and most of them have π-conjugated electronic structures, whereas less conductive molecules consist mainly of C-C σ bonds and show larger λ values [24-27, 39, 41]. The advent of theoretical calculations explains the correlation between the molecule conductances and the electronic structures [44-51]. The combination of none-equilibrium Green function method with first-principles density functional theory (DFT) calculations provides the transport characteristics of a single molecule. The theoretical studies have revealed that the electronic states of the molecule near E_F of the electrodes dominantly carry the electrical current as transport channels in the SMJ. In particular, the highest occupied molecular orbitals (HOMOs) and lowest unoccupied molecular orbitals (LUMOs) are dominant contributors to the electron transport through the SMJ. When the HOMO-LUMO gap is larger, the constant λ is larger so that the molecule is less conductive. In addition to the molecule electronic structure, the coupling of the anchoring group with the electrodes also plays a role. The dependence of conductance on the anchoring groups has been investigated systematically for benzene derivatives [28, 31]. The conductances are 0.004 G_0, 0.003 G_0 and 0.01 G_0 for Au-S-C_6H_6-S-Au, Au-NC-C_6H_6-CN-Au and Au-$_2$HNS-C_6H_6-NH_2-Au junctions. The conductance increases as the anchoring group changes from -S- and -CN- to -NH_2-. This tendency is reversed for the Pt electrodes. The conductances of Pt-S-C_6H_6-S-Pt and Pt-NC-C_6H_6-CN-Pt junctions are 0.03 G_0 which is ten times larger than those of the Au junctions, while the conductance of Pt-$_2$HN-

C_6H_6-NH_2-Pt is much smaller, 0.005 G_0. These examples clearly indicate that the combination of anchoring group with the electrode material plays an important role.

3.1 Determination of number of transport channels and the transmission probabilities

Both MCBJ and STM enable us to experimentally evaluate the conductance of a single molecule. Measuring the conductance, however, is insufficient to fully understand the electron transport through a single molecule. We must answer the following questions:

- How many molecular orbitals are relevant of the transport?
- What correlation is observed between the number of relevant orbitals and the one electron energy spectrum of the molecule?
- What factors govern the relative contributions of the relevant orbitals to the total conductance?
- What happens to the total conductance and the relevant orbitals when the molecule configuration changes in the junction?

The determination of number of transport channels and transmission probabilities (n and τ_i) enables us to answer the questions, to get much deeper insights on the physics underlying the electron transport through a single molecule, and finally to realize a breakthrough leading to the fabrication of single molecule devices. These parameters are inherent to a molecule in the junction like a PIN (Personal Identification Number) code. Although it is not easy to determine experimentally n and τ_i, two techniques have been reported for the purpose; one is measurement of shot noise and the other measurement of multiple Andreev reflections (MARs). These two techniques are described in the following subsections.

3. 1. 1 Shot noise measurement

There are two kinds of intrinsic sources for noise emerging in the electrical current through a conductor [52]. One is thermal fluctuation in the occupation number of the states in the conductor and the other stems from the quantization of the electrical charge. The former leads to thermal noise and the latter gives rise to shot noise. At none-zero temperature, electrons in the conductor are excited thermally into the unoccupied states and the average occupation number of each state is determined by the Fermi-Dirac distribution function. The mean squared fluctuation of the occupation number does not vanish at none-zero temperature, giving rise to the thermal noise [52]. In contrast, the origin of shot noise is totally different. Now, we consider virtually only one particle incident to a potential barrier. The particle transmits

through the barrier with certain transmission probability τ or it is reflected by the barrier with the probability of $1-\tau$. The potential barrier partitions the incident particle beam into transmitted or reflected beam. Considering the occupation numbers of the "transmitted" or "reflected" states that the particle takes, this partitioning fluctuates these numbers, which leads to the shot noise [52]. In the limiting case where the barrier is completely transparent, the particle always transmits and the occupation number of "transmitted" state is always 1 with zero occupation in the "reflected" state. As a consequence, the shot noise does not emerge because the partitioning does not take place. This is true for the case that the barrier always reflects the particle. For the intermediate case, the partitioning causes the shot noise. Therefore, measuring the shot noise of electrical current through the conductor offers a route to evaluate the transmission probability. According to quantum statistics, the shot noise power S_I from a transport channel is expressed as $S_I = 2eVG_0\tau(1-\tau)$. Including the finite temperature (T) effect and n transport channels, S_I is described as

$$S_I = G_0\left\{eV\coth\left(\frac{eV}{2k_BT}\right)\sum_{i=1}^{n}\tau_i(1-\tau_i) + 2k_BT\sum_{i=1}^{n}\tau_i^2\right\} \quad (6)$$

where k_B is the Boltzmann constant [52]. In the limit of low temperature where $k_BT \ll eV$, the equation reduces to

$$S_I = 2eI\left(\frac{\sum_{i=1}^{n}\tau_i(1-\tau_i)}{\sum_{i=1}^{n}\tau_i}\right) = 2eI\,F(\tau_1,\cdots,\tau_n). \quad (7)$$

Here, F is called as Fano factor that describes the contribution of each transport channel to the noise power. Based on the eqs. (6) and (7), we can determine n and τ_i by measuring the shot noise.

The challenges to determine n and a set of τ_i $(i = 1, 2, \cdots, n)$ have been done for a few molecules by measuring the shot noise with MCBJ. Ruitenbeek and coworkers analyzed the shot noise with the eqs. (6) and (7), and successfully determined these quantities for the SMJs of H_2 [29], H_2O [34] and C_6H_6 [36] bridging Pt electrodes. The H_2-SMJ has a conductance close to $1G_0$. This value is explained by a dominant transport channel with additional channels which transmission probabilities are very small. The conductance of the H_2O-SMJ ranges from $0.5G_0$ to ~$1G_0$. These values are explained by a single dominant channel. In contrast, multiple channels contribute to the electron transport through a C_6H_6 molecule. The conductance depends on the configuration of C_6H_6 in the junction and three conductance values are observed; $0.2G_0$, $0.71G_0$ and $1.08G_0$. These values are decomposed into a single channel, three channels and two channels, respectively. They carried out the DFT calculations for the possible various configurations of a C_6H_6 molecule inside the junction, and suggested that the number of the

channels is correlated with the number of C atoms bonded to the Pt atom at each electrode.

3. 1. 2 MARs measurement

Here we compare the I-V characteristics of normal conductor/vacuum/superconductor (N/V/S), S/V/S, N/S and S/N/S junctions and describe multiple Andreev reflections (MARs). Fig. 4 summarizes the I-V characteristics of N/V/S, S/V/S and N/S junctions [53]. We hereafter assume that (i) the normal conductor has a simple band structure which density of states (DOS) is approximately constant around E_F, (ii) the superconductor shows a superconducting gap and has a DOS spectrum described by the Dynes function [54],

$$D(E, \Delta, \Gamma) = \mathrm{Re}\left[\frac{E - i\Gamma}{\sqrt{(E - i\Gamma)^2 - \Delta^2}}\right] \quad (8)$$

where Δ is a superconducting gap energy and Γ is a broadening parameter, and (iii) the temperature is absolute zero so that the thermal excitation of electrons is prohibited. In addition, we assume that the superconducting gaps of both superconductors in the S/V/S and S/N/S junctions are identical to Δ. Consider the current flowing through each junction by applying bias voltage across the junction. For the N/V/S junction, an electron (hole) cannot enter into the superconductor as long as the voltage meets the condition of $|V| < \Delta/e$. Once $|V|$ exceeds Δ/e, the current flows. The first derivative of the current as a function of V, the dI/dV spectrum, reflects the DOS spectrum of the superconductor as shown in Fig. 4 (a). Similar I-V spectrum is observed for the S/V/S junction as shown in Fig. 4 (b). For this junction, a gap appearing in the spectrum is not 2Δ but 4Δ. The dI/dV spectrum reflects the convolution of the DOS spectra of two superconductors.

In contrast, the N/S junction shows a totally different I-V spectrum [see Fig. 4 (c)] because the Andreev reflection occurs at the N/S interface. Fig. 5 displays the schematic illustration of the Andreev reflection [55]. Consider a case that an electron with the energy smaller than the superconducting gap is incident to the N/S interface. Since there are no electronic states available for the incident electron inside the superconducting gap, the electron cannot enter into the superconductor and is reflected at the N/S interface [Fig. 5 (b)]. This is the normal reflection. In the Andreev reflection, the incident electron couples another electron in the normal conductor to form a Cooper pair and enters the superconductor, and simultaneously a created hole is reflected into the normal conductor as shown in Figs. 5 (c) and (d). The same process takes place for a hole entering the superconductor. An incident hole forms a Cooper pair to enter into the superconductor with the reflection of an electron. The probability that the Andreev

reflection occurs depends on the potential barrier at the N/S interface [56]. When the N/S interface is clean and the electronic structures are smoothly connected at the interface, the probability of the Andreev reflection is 1. In addition, since an incident electron (or hole) enters the superconductor as a Cooper pair, the charge carried by this process is twice as much as that carried by the normal transport process. As a result, the conductance in the voltage range of $|V| < \Delta/e$ is twice as large as that in the region of $|V| \geq \Delta/e$ [see Fig. 4 (c)].

In the S/N/S junction, the Andreev reflection takes place repeatedly at both S/N and N/S interfaces until the Andreev-reflected electron or hole reaches a normal electronic state in either of the superconductors [53, 57-59]. Consequently, the electrical current flows across the junction even for $|V| < 2\Delta/e$. Characteristic structures called as subharmonic gap structures (SGSs) emerge inside the superconducting gap in the I-V and dI/dV spectra of the S/N/S junction. This feature contrasts to the S/V/S junction. The sequence of the Andreev reflections is called as multiple Andreev reflections (MARs). Fig. 6 illustrates schematically the quasi-classical picture of the MARs. Consider the current flowing at the bias voltage of $2\Delta/2 < eV < 2\Delta/1$ as an example. The current flows via a single Andreev reflection as shown in Fig. 6 (b). An electron is incident from the right superconductor to the left N/S interface where the Andreev reflection occurs, and a hole is reflected, which enters and occupies a normal electronic state in the right superconductor. Figs. 6 (c) and (d) display the current paths via two-fold and three-fold Andreev reflection processes, respectively. The bias voltages are $2\Delta/3 < eV < 2\Delta/2$ and $2\Delta/4 < eV < 2\Delta/3$, respectively. In the two-fold Andreev reflection process [see Fig. 6 (c)], an incident electron from the right superconductor enters the left superconductor by forming a Cooper pair and simultaneously a hole left by this process is reflected to the right superconductor. Then, this hole forms a Cooper pair at the right N/S interface with the generation of an electron, which has sufficient energy to overcome the superconducting gap and reaches the unoccupied normal electronic state of the left superconductor. The similar sequences take place for the three-fold process and a hole finally reaches the occupied state of the right superconductor [see Fig. 6 (d)]. As these examples demonstrate, a transport path switches from the $(\eta + 1)$-fold reflection process to the η-fold one, every time the bias voltage exceeds the value of $eV = 2\Delta/(\eta + 1)$, where $\eta\ (= 1, 2, \cdots)$ is the number of Andreev reflections. Therefore, the current carried by a single transport channel with the transmission probability of τ is obtained by summing up the contributions from the η-fold reflection processes $\eta\ (= 1, 2, \cdots)$ and is expressed as

$$I_i(\tau, V) = \sum_{\eta=1}^{\infty} \theta(\eta eV - 2\Delta)\tau^{\eta} K_{\eta}(\tau, V) \quad (9)$$

where θ is the Heaviside step function and $K_{\eta}(\tau, V)$ describes the current component carried by the η-fold Andreev reflection process [59]. Fig. 7 shows the calculated I-V spectra as a function of τ. Every time the voltage passes through $2\Delta/(\eta+1)e$ $(\eta = 1, 2, \cdots)$, the current logarithmically increases in the stepwise manner because the current derived from the η-fold reflection process is proportional to τ^{η}. As clearly demonstrated by Fig. 7, the spectra depend strongly on τ. When τ is close to 1, the current paths derived from the higher-order Andreev reflections lead to the sizable SGSs in the I-V spectrum. Decreasing τ, the SGSs are reduced drastically and the spectrum gradually approaches that of the S/V/S junction.

Extending the above discussion to the case that the S/N/S junction has multiple transport channels, the total current across the junction is the sum of the contributions from these channels as follows:

$$I_{total} = \sum_{i=1}^{n} I_i(\tau_i, V) \quad (10)$$

where n is the number of channels and τ_i is the transmission probability of the i-th channel. The strong nonlinearity of the I-V spectrum as functions of n and a set of τ_i $(i = 1, 2, \cdots, n)$ enables us to determine these quantities of the S/N/S junction by fitting the measured I-V spectrum with the eqs. (9) and (10).

The determination of n and τ_i by means of the MARs measurement has not been done for SMJ yet but it has been made successfully for atomic point contacts [60-62]. Scheer et al. [61] have fabricated the atomic contacts of Al and Pb by using STM, measured the I - V characteristics of the superconducting atomic contacts at 1.5 K and analyzed the SGSs with the eqs. (9) and (10). They demonstrated that two or three channels are responsible to the conductance, and revealed that the valence orbitals, i.e., s and p orbitals, work as the channels.

4. Electron transport through a single C_{60} molecule

This section focuses on the electron transport characteristics of a single C_{60} molecule mainly based on our MARs measurements of a C_{60}-SMJ constructed from superconducting electrodes by using STM [63]. We describe the fabrication of the SMJ with STM, the conductance measurement, and the determination of n and a set of τ_i through the MARs measurements in the following subsections, and we discuss the transport characteristics with the electronic and geometrical structures of C_{60} in the junction.

4. 1 Fabrication of a C_{60}-SMJ and conductance measurement with STM

In our experiment, a C_{60}-SMJ was fabricated by contacting a STM tip constructed from a Nb wire with a C_{60} molecule deposited on a clean Pb(111) substrate. A Nb wire was used for an STM tip and a Pb(111) single crystal surface as a counter electrode. These superconducting electrodes sandwich a single C_{60} molecule.

A superconducting STM tip was prepared by cutting a Nb wire mechanically in ultrahigh vacuum condition in order to avoid the oxidation of Nb and to preserve the superconductivity [64]. The superconductivity of the Nb tip was characterized by measuring the STS spectra with a Au(111) clean surface. Nearly free electron state exists on the Au(111) surface [65], which DOS spectrum is almost flat around the E_F. Thus, the measured STS spectrum reflects the superconductivity of the Nb tip.

The Pb(111) substrate was cleaned by repeated cycles of Ar^+ ion sputtering and annealing. The clean surface was characterized by using STM. Figs. 8 (a) and (b) show topographic images of the clean Pb(111) surface. Atomically flat surface is obtained and the lines running from the top to the bottom are single-atom steps [Fig. 8 (a)]. In the flat terraces, a hexagonal array of protrusions is observed as shown in Fig. 8 (b). The distance between the protrusions is 0.35 nm, which matches the lattice constant of the Pb(111) surface. Figs. 8 (c) and (d) show the STS spectra measured at the terrace. The wide range spectrum is featureless, indicating the simple DOS of Pb derived mainly from the s and p electrons. In the narrow range spectrum [Fig. 8 (d)], quasi-particle peaks appear symmetrically with respect to E_F, and a superconducting gap opens. The spectral shape is nicely reproduced with the eq. (8) and it is well fitted with $\Delta = 1.36$ meV and $\Gamma = 0.15$ meV. The gap energy of $\Delta = 1.36$ meV is in good agreement with that of the bulk (1.36 meV). The broad peaks at $V = \pm 5$ mV stem from the inelastic excitations of the phonon of Pb [64].

Fig. 9 shows an STM topographic image of the Pb(111) surface partially covered with C_{60} molecules. Each bright round shape is a single C_{60} molecule, and the molecules form a hexagonal array. The lattice constant of the array is approximately 1.0 nm, which well accords with the previous STM study about the adsorption of C_{60} on Pb(111) [66]. Taking a close look at the STM image, the C_{60} molecules at the edge of the array emerge as two different shapes; round and two-lobed shapes. Hereafter, we call the round and two-lobed shape molecules as α- and β-type molecules, respectively. The shape observed by STM is correlated directly with the spatial distribution of the molecular orbitals and we can identify the molecular orientation from the STM image. According to the previous studies, the LUMOs of C_{60}

provide dominant paths around E_F for the electron tunneling [67,68]. The STM image reflects the spatial distributions of the LUMOs. Thus, we imply the molecular orientations from the STM images as follows: the α-type molecule is bonded to Pb(111) through one of the pentagonal rings so that the pentagonal ring faces towards the vacuum, while the β-type molecule is adsorbed through a single carbon atom and the node appears in the image. As a result, these molecules appear as different shapes. The favorable adsorption configurations of both types of molecules are schematically shown in Fig. 9 (b).

The conductance measurement of a single C_{60} molecule with STM was performed in the same manner mentioned above [see Fig. 3 (b)]. At first, we take a topographic image of the surface partially covered with the C_{60} molecules and confirm the position of a target C_{60} molecule in the STM image. Secondly, we set the horizontal position of the STM tip above the target. Thirdly, we turn off the feedback loop and approach the STM tip towards the target by controlling the vertical position of the STM tip with the measurement of the current flowing across the junction as a function of the distance between the tip and the target. When the tip contacts with the target, we stop approaching the tip and retract the tip to the original position. Finally, we measure a topographic image and confirm that the target molecule, substrate and the tip are not damaged. In addition, we measured *I*-*V* spectra at certain positions of the tip relative to the target molecule.

Figs. 10 (a) and (b) show typical conductance traces called *G*-*Z* curves, where *Z* is the moving distance of the tip from the original position. When the tip approaches to the molecule, *Z* increases. The *G*-*Z* curve in Fig. 10 (a) shows the successful formation of the SMJ without causing any damage to both tip and sample, which are confirmed by acquiring an STM image after the measurement. As *Z* increases, *G* initially increases in a logarithmic manner because the vacuum tunneling occurs. Then the slope of the *G*-*Z* curve gradually changes at around $G = 0.2\ G_0$ and *G* asymptotically reaches a saturated value. When the tip is retracted, the *G*-*Z* curve traces almost the same one taken when the tip approaches the molecule. In contrast, the *G*-*Z* curve in Fig. 10 (b) shows a typical result observed when the tip crashed into the sample surface. As the tip approaches the target molecule, *G* increases similarly to the successful case, but it suddenly jumps to exceed $0.5\ G_0$. The conductance jump happens because the tip crashed into the surface to destroy the molecular array as shown in the STM image taken after the crash [compare the STM images in Figs. 10 (c) and (d)]. The *G*-*Z* curve fluctuates severely and shows a high conductance value when the tip is retracted after the crash as shown in Fig. 10 (b) with the pink curve. This feature indicates that an atomic wire is formed by the tip and the substrate atoms and it is broken partially upon the tip retraction. Whenever $G < 0.5\ G_0$, the *G*-*Z* curves almost overlap each other

upon approaching and retracting the tip and the STM images taken before and after the contact measurement are essentially the same. The condition of $G < 0.5\ G_0$ guarantees that the SMJ is successfully formed without damaging both tip and sample. We determined the conductance of the C_{60} molecule to be ~0.3 G_0. The conductance of a single C_{60} molecule has been measured previously [32, 33, 35, 37, 38, 41]. The conductances of the C_{60}-SMJs of Au, Ag and Pt electrodes were determined to be 0.3, 0.5 and 0.7 G_0 [33, 35, 38, 41]. In addition, the STM contact measurements performed for C_{60} on Cu substrate have reported ~ 0.2 G_0 [32, 37]. The value of ~0.3 G_0 is comparable to these previous results.

4.2 MARs through a C_{60} molecule and the determination of n and τ_i $(i = 1, 2, \cdots, n)$

Fig. 11 shows four *I-V* spectra of four junctions acquired at T = 400 mK. The *I-V* spectra taken for the SMJ of the α- and β-type C_{60} molecules are presented in Figs. 11 (a) and (b), respectively. Figs. 11 (c) and (d) show the *I-V* spectrum of a atomic-sized junction formed by contacting the Nb tip directly to the bare Pb(111) substrate and that of a tip-vacuum-substrate tunnel junction (i.e., the conventional STM geometry), respectively. In Fig. 11 (d), the almost zero current below 2 mV indicates the superconducting gap. In contrast to Fig. 11 (d), step-like increases marked by arrows appear inside the superconducting gap region (V < 3 mV) as shown in Figs. 11 (a)- (c). These fine structures are the SGS produced by two- and three-fold MARs. The dotted vertical lines at V = 3 mV ($eV = 2\Delta = \Delta_{\mathrm{tip}} + \Delta_{\mathrm{substrate}}$) indicate the border separating both inside and outside of the superconducting gap. The current increases linearly with voltage outside the gap. The red curves in Figs. 11 (a)-(c) are the best fits calculated with the eq. (10). The calculated curves reproduce the experimental data quite well with $n = 3$ for (a) and (b) and with $n = 4$ for (c). For reference, we also show the curves calculated for $n = 1$ and $n = 2$ in Fig. 11 (a). These curves do not reproduce the experimental result, especially, the SGSs derived from the MARs, indicating that al least three transport channels are necessary. One might think that the fitting quality should be more improved with assuming more channels. Since the sum of τ_i $(i = 1, 2, \cdots, n)$ is equal to G/G_0 according to the Landauer formula, the transmission probabilities of the channels except for the dominant ones are very small and can be neglected. Consequently, fitting the *I-V* characteristic derived from the MARs with the eq. (10) provides the physically reasonable number of the transport channels. Thus, we determine n and a set of $\{\tau_i\}$ uniquely for the junctions as follows: $n = 3$ and τ_i = {0.095 ± 0.03, 0.095 ± 0.03, 0.095 ± 0.03} for the molecular junction of the α-type molecule; $n = 3$ and τ_i = {0.17 ± 0.02. 0.075 ± 0.02, 0.06 ± 0.02} for the β-type molecule; $n = 4$ and τ_i = {0.10 ± 0.03, 0.09 ±

0.03, 0.09 ± 0.03, 0.09 ± 0.03} for the atomic-sized junction. Here we assumed that both superconducting electrodes have an identical gap of $\Delta = \frac{\Delta_{\mathrm{tip}} + \Delta_{\mathrm{substrate}}}{2}$ (=1.5 meV). We also assumed a BCS-type DOS spectrum without the lifetime smearing of the electronic structure for each superconducting electrode. Although the asymmetry of the electrodes and the broadening effects were ignored in the analysis, we have successfully reproduced the experimental results and determined n and a set of $\{\tau_i\}$ for the two types of C_{60}-SMJs with a sufficient accuracy.

The STS spectra of the α- and β-type molecules provide the origin of the transport channels and the determined number of the channels (n = 3). Fig. 12 shows the STS spectra taken for the α- and β-type molecules. The peaks around 100 ~ 200 mV are derived from the LUMOs of the C_{60} molecule which are originally triply-degenerate in the gas phase [69]. The degeneracy is partially lifted by the molecule-substrate interactions. In contrast, the peaks associated with the occupied MOs do not appear in the measured energy range from -1.5 to 0 V, indicating that the molecular resonances derived from the occupied MOs lie about 1.5 eV deeper below E_F [70, 71]. The increase of the spectral intensity observed at -1.5 eV reflects the tails of the molecular resonances, but the spectral intensities of the tails are negligibly small at E_F. These features indicate that the molecular resonances derived from the LUMOs are responsible for the electronic transport through the C_{60} molecule while the contributions from the occupied MOs are negligible. The total number of transport channels (n = 3) matches quite nicely with that of the LUMOs. In fact, it has been theoretically reported that the LUMOs of C_{60} provide the dominant routes for electronic transport through a C_{60} molecule sandwiched by metal electrodes [72, 73]. The STS spectra do not strictly represent the electronic structure of the SMJ because the STS spectra are measured in the vacuum tunneling regime. However, we believe that the electronic structure does not change significantly by bringing the tip into contact with the molecule. Hence, we have concluded that, not only the determined number of transport channels is valid, but also our results fully justify the theoretical prediction that the number of MOs near E_F determines that of dominant channels [49].

Next, let us examine the relation between transmission probabilities and molecular orientation. Interestingly, the transmission probabilities of the α-type molecule are different from those of the β-type molecule despite the fact that these molecules show very similar STS spectra. Each transmission probability of the α-type molecule is almost identical; consequently, the three channels equally contribute to the total conductance. In contrast, transmission probability of a channel is larger than the others for the β-type molecule, making the channel dominant contributor to the total conductance. At present, we do not have a definitive and quantitative explanation on the relation between the transmission

probabilities and the molecular orbitals. However, we can provide a reasonable guess for the different transmission probabilities from the viewpoint of molecular orientations. While the contact point for the α-type molecule is the pentagonal ring around which three LUMO states spread uniformly, the point for the β-type is the C atom at which a node of the LUMO is located. The spatial distribution of the MO responsible for the electronic transport relative to the electrode thus determines the magnitude of the transmission probability of the dominant channel. Theory based on the non-equilibrium Green function technique demonstrates that the transmission of the SMJ can be represented by

$$\tau(E) = \frac{1}{2}\sum_{k}\frac{(2\pi\beta^2\rho_F C_{rk}C_{sk}^*)^2}{(E-\varepsilon_k)^2+\delta_k^2} \quad (11)$$

where β is a hopping integral between the metal electrode and MO specified with k, C_{rk} and C_{sk}^* are the coefficients of k-th MO at r and s sites inside the molecular junction, ε_k represents the energy of the k-th MO, and δ_k is an infinitesimal constant which determines the width of the MO caused by the molecule-electrode coupling [45, 51]. The eq. (11) indicates that τ depends strongly on the configuration of C_{60} molecule in the SMJ and the place where the tip contacts inside the molecule. The combination of the eq. (11) with the DFT calculations of C_{60} on Pb(111) may reveal the origin of the difference between the α- and β-type C_{60} molecules.

5. Summary and outlook

Electron transport through a single molecule is an attractive issue in the broad spectrum of scientific fields from molecular physics, physical chemistry, analytical chemistry, organic chemistry to biochemistry. It is also important from the technological points of view to overcome the various problems involved in the current semiconductor technology. The progress in both experimental and theoretical techniques enables us to evaluate the conductance of a single molecule and discuss the transport mechanism from the electronic and geometric structures of a molecule in SMJ.

In this chapter, we described the determination of n and τ_i of SMJ. We determined these quantities for two types of the C_{60}-SMJs (α- and β-type molecules) by means of the MARs measurements with STM. Three transport channels equally contribute to the conductance for the α-type molecule while the conductance of the β-type molecule is determined by one dominant and two additional channels. These channels come from the LUMOs and the transmission probabilities depend on the molecule configurations, i.e., the spatial distributions of the LUMOs. These results provide a good example that the determination of n and τ_i enables us to fully understand the transport mechanism

through a single molecule. Actually, the determination of n and τ_i has been limited to only several molecules that we described above. More molecules remain to be evaluated. In particular, the magnetic SMJs where ferromagnetic electrodes sandwich a nonmagnetic or a magnetic molecule are intriguing targets. The role of STM, which is capable of visualizing the molecule configuration on a metallic electrode and identifying the molecular state through the measurement of the electronic, vibrational and spin spectra, becomes increasingly important in this field.

Acknowledgements

We gratefully acknowledge the support for this work by Grant-in-Aid for Scientific Research on Innovative Areas “Molecular Architectonics: Orchestration of Single Molecules for Novel Functions” (Grant Number 25110008).

References

[1] W. F. Brinkman, D. E. Haggan and W. W. Troutman, IEEE J. Solid State Circuits, **32**, 1858 (1997).

[2] *Chips 2020 A Guide to the Future of Nanoelectronics*, Ed. B. Hoefflinger, Springer, Berlin 2012.

[3] The ITRS2013 report is available at the following URL: http://www.itrs2.net/.

[4] L. Bogani, and W. Wernsdorfer, Nat. Mater. **7**, 179 (2008).

[5] A. Aviram, and M. A. Ratner, Chem. Phys. Lett. **29**, 277 (1974).

[6] P. K. Misra, Physics of Condensed Matter, Elsevier, New York (2012).

[7] R. Landauer, IBM J. Research and Development **1**, 223 (1957).

[8] R. Landauer, J. Phys.: Condens. Matter **1**, 8099 (1989).

[9] Y. Imry, and R. Landauer, Reviews of Modern Physics **71**, S306 (1999).

[10] S. Datta, *Electronic Transport in Mesoscopic Systems*, Cambridge University Press, Cambridge, 2003.

[11] C. J. Muller, J. M. van Ruitenbeek, and L. J. de Jongh, Physica C **191**, 485 (1992).

[12] J. M. van Ruitenbeek, A. Alvarez, I. Piñeyro, C. Grahmann, P. Joyez, M. H. Devoret, D. Esteve and C. Urbina, Rev. Sci. Instrum. **67**, 108 (1996).

[13] R. H. M. Smit, Y. Noat, C. Untiedt, N. D. Lang, M. C. van Hemert and J. M. van Ruitenbeek, Nature **419**, 906-909 (2002).

[14] L. H. Yu, Z. K. Keane, J. W. Ciszek, L. Cheng, M. P. Stewart, J. M. Tour and D. Natelson, Phys. Rev. Lett. **93**, 266802 (2004).

[15] J. A. Stroscio, R. M. Feenstra, and A. P. Fein, Phys. Rev. Lett. **57**, 5 (1986).

[16] R. M. Feenstra, J. A. Stroscio, and A. P. Fein, Surf. Sci. **181**, 295 (1987).

[17] B. C. Stipe, M. A. Rezaei, and W. Ho, Science **280**, 1732 (1998).

[18] W. Ho, J. Chem. Phys. **117** 11033 (2002).

[19] A. J. Heinrich, J. A. Gupta, C. P. Lutz and D. M. Eigler, Science **306**, 466 (2004).

[20] N. Tsukahara, K. Noto, M. Ohara, S. Shiraki, N. Takagi, J. Miyawaki, M. Taguchi, A. Chainani, S. Shin, M. Kawai, Phys. Rev. Lett. **102**, 167203 (2009).

[21] C. J. Muller, B. J. Vleeming, M. A. Reed, J. J. S. Lamba, R. Hara, L. Jones, and J. M. Tour, Nanotechnology **7**, 409 (1996).

[22] M. A. Reed, C. Zhou, C. J. Muller, T. P. Burgin, and J. M. Tour, Science **278**, 252 (1997).

[23] B. Xu and N. J. Tao, Science **301**, 1221 (2003).

[24] X.Xiao, B.Xu, N.J.Tao, J. Am. Chem. Soc. **126**, 5370 (2004).

[25] J. He, F. Chen, J. Li, O. F. Sankey, Y. Terazono, C. Herrero, D. Gust, T. A. Moore, A. L. Moore, S. M. Lindsay, J. Am. Chem. Soc. **127**, 1384 (2005).

[26] N. J. Tao, Nat. Nanotechnol. **1,** 173 (2006).

[27] F. Chen, X. Li, J. Hihath, Z. Huang, N. Tao, J. Am. Chem. Soc. **128**,15874 (2006).

[28] M. Kiguchi, S. Miura, K. Hara, M. Sawamura, K. Murakoshi, Appl. Phys. Lett. 89, 213104 (2006).

[29] D. Djukic, and J. M. van Ruitenbeek, Nano Lett. **6,** 789 (2006).

[30] L. Venkataraman, J. E. Klare, C. Nuckolls, M. S. Hybertsen, M. L. Steigerwald, Nature **442**, 904 (2006).

[31] M. Kiguchi, S. Murata, K. Hara, M. Sawamura, K. Murakoshi, Appl. Phys. Lett. **91**, 053110 (2007).

[32] N. Néel, J. Kröger, L. Limot, T. Frederiksen, M. Brandbyge, and R. Berndt, Phys. Rev. Lett. **98**, 065502 (2007).

[33] T. Böhler, A. Edtbauer, E. Scheer, Phys. Rev. B **76**, 125432 (2007).

[34] O. Tal, M. Krieger, B. Leerink, and J. M. van Ruitenbeek, Phys. Rev. Lett. **100**, 196804 (2008).

[35] M. Kiguchi and K. Murakoshi, J. Phys. Chem. C **112**, 8140 (2008).

[36] M. Kiguchi, O. Tal, S. Wohlthat, F. Pauly, M. Krieger, D. Djukic, J. C. Cuevas, and J. M. van Ruitenbeek, Phys. Rev. Lett. **101**, 046801 (2008).

[37] M. Kiguchi, Appl. Phys. Lett. **95**, 073301 (2009).

[38] G. Schull, T. Frederiksen, A. Arnau, D. Sánchez-Portal, and R. Berndt, Nat. Nanotechnol. **6**, 23 (2011).

[39] G. Sedghi, V. M. García-Suµrez, L. J. Esdaile, H. L. Anderson, C. J. Lambert, S. Martín, D. Bethell, S. J. Higgins, M. Elliott, N. Bennett, J. E. Macdonald, R. J. Nichols, Nat. Nanotechnol. **6**, 517 (2011).

[40] H. Vazquez, R. Skouta, S. Schneebeli, M. Kamenetska, R. Breslow, L. Venkataraman and M. S. Hybertsen, Nat. Nanotechnol. **7**, 663 (2012).

[41] M. Kiguchi, and S. Kaneko, ChemPhysChem. **13**, 1116 (2012).

[42] D. Xiang, H. Jeong, T. Lee and D. Mayer, Adv. Mater. **25**, 4845 (2013).

[43] M. Magoga and C. Joachim, Phys. Rev. B **56**, 4722 (1997).

[44] J. Heurich, J. C. Cuevas, W. Wenzel and G. Schön, Phys. Rev. Lett. **88**, 256803 (2002).

[45] T. Tada and K. Yoshizawa, ChemPhysChem **3**, 1035 (2002).

[46] A. Nitzan, and M. A. Ratner, Science **300**, 1384 (2003).

[47] G. C. Solomon, A. Gagliardi, A. Pecchia, T. Frauenheim, A. D. Cario, J. R. Reimers and N. S. Hush, Nano Lett. **6**, 2431 (2006).

[48] M. Paulsson, M. Brandbyge, Phys. Rev. B 76, 115117 (2007).

[49] J. P. Bergfield, J. D. Barr, and C. A. Stafford, ACS Nano **5,** 2707 (2011).

[50] E. Lörtscher, B. Gotsmann, Y. Lee, L. Yu, C. Rettner, and H. Riel, ACS Nano **6**, 4931 (2012).

[51] K. Yoshizawa, Acc. Chem. Res. **45**, 1612 (2012).

[52] Y. M. Blanter and M. Büttiker, Phys. Rep. **336**, 1 (2000).

[53] M. Tinkham, *Introduction to superconductivity*, Dover, New York, 2004.

[54] R. C. Dynes, V. Narayanamurti, J. P. Garno, Phys. Rev. Lett. **41**, 1509 (1965).

[55] A. Andreev, Sov. Phys. JETP **19**, 1228 (1964).

[56] G. E. Blonder, M. Tinkham, T. M. Klapwijk, Phys. Rev. B **25,** 4515 (1982).

[57] T. M. Klapwijk, G. E. Blonder, M. Tinkham, Physica **109 & 110B**, 1657 (1982).

[58] M. Octavio, M. Tinkham, G. E. Blonder, T. M. Klapwijk, Phys. Rev. B **27**, 6739 (1983).

[59] E. N. Bratus, V. S. Shumeiko, and G. Wendin, Phys. Rev. Lett. **74**, 2110 (1995).

[60] E. Scheer, P. Joyez, D. Esteve, C. Urbina, and M. H. Devoret, Phys. Rev. Lett. **78**, 3535 (1997).

[61] E. Scheer, N. Agrait, J. C. Cuevas, A. L. Yeyati, B. Ludoph, A. M. Rodero, G. R. Bollinger, J. M. van Ruitenbeek, and C. Urbina, Nature **394**, 154 (1998).

[62] B. Ludoph, N. van der Post, E. N. Bratus, E. V. Bezuglyi, V. S. Shumeiko, G. Wendin, and J. M. van Ruitenbeek, Phys. Rev. B **61,** 8561 (2000).

[63] R. Hiraoka, R. Arafune, N. Tsukahara, M. Kawai, N. Takagi, Phys. Rev. B **90**, 241405(R) (2014).

[64] O. Naaman, W. Teizer, and R. C. Dynes, Rev. Sci. Instru. **72**, 1688 (2001).

[65] W. Chen, V. Madhavan, T. Jamneala, and M. F. Crommie, Phys. Rev. Lett. **80**, 1469 (1998).

[66] H. I. Li, K. J. Franke, J. I. Pascual, L. W. Bruch, and R. D. Diehl, Phys. Rev. B **80**, 085415 (2009).

[67] J. I. Pascual, J. Gómez-Herrero, D. Sánchez-Portal, H. -P. Rust, J. Chem. Phys. **117**, 9531 (2002).

[68] X. Lu, M. Grobis, K. H. Khoo, S. G. Louie, and M. F. Crommie, Phys. Rev. B **70**, 115418 (2004).

[69] M. R. Savina, L. L. Lohr, and A. H. Francis, Chem. Phys. Lett. **205**, 200 (1993).

[70] I. F. Torrente, K. J. Franke, and J. I. Pascual, J. Phys. Condens. Matter **20**, 184001 (2008).

[71] G. Schulze, K. J. Franke, and J. I. Pascual, New J. Phys. **10**, 065005 (2008).

[72] J. Taylor, H. Guo, and J. Wang, Phys. Rev. B **63**, 121104 (2001).

[73] N. Kobayashi, T. Ozaki, K. Tagami, M. Tsukada, and K. Hirose, Jpn. J. Appl. Phys. **45**, 2151 (2006).

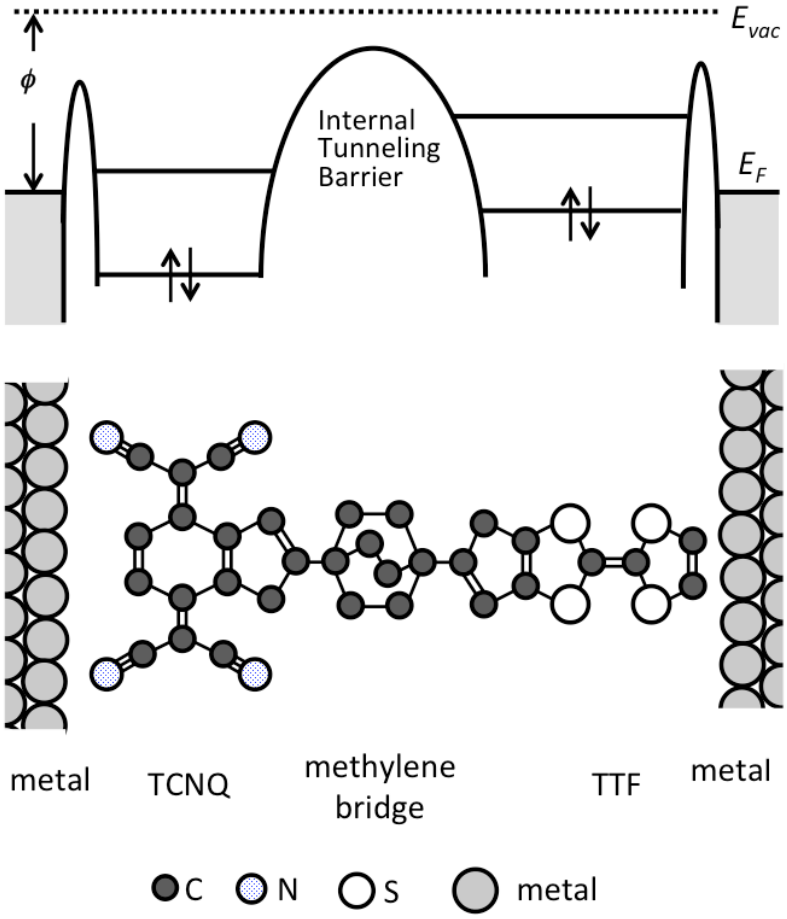

Fig. 1 Electronic and geometrical structures of a single molecule rectifier [5]. The molecule consisting of tetracyanoquinodimethane (TCNQ), tetrathiafulvalene (TTF) and a methylene bridge connects two metallic electrodes. The methylene bridge isolates the TCNQ and TTF molecules electronically so that the entire electronic structure is asymmetric, leading to rectification functionality. All the hydrogen atoms are omitted for clarity.

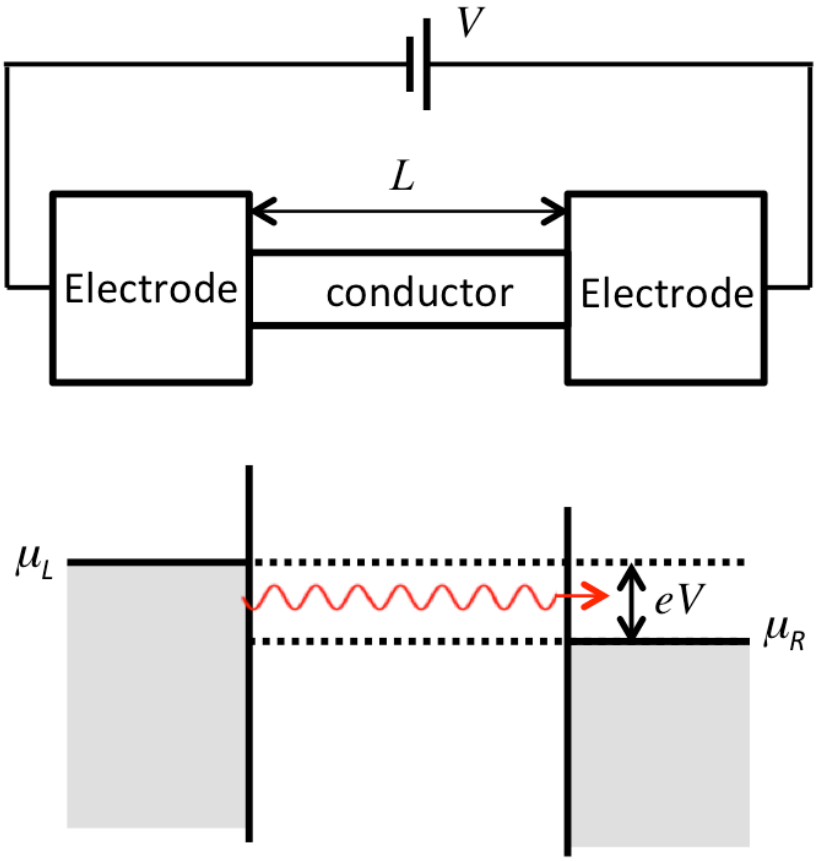

Fig. 2 Electron transport through a one-dimensional nanoscale conductor.

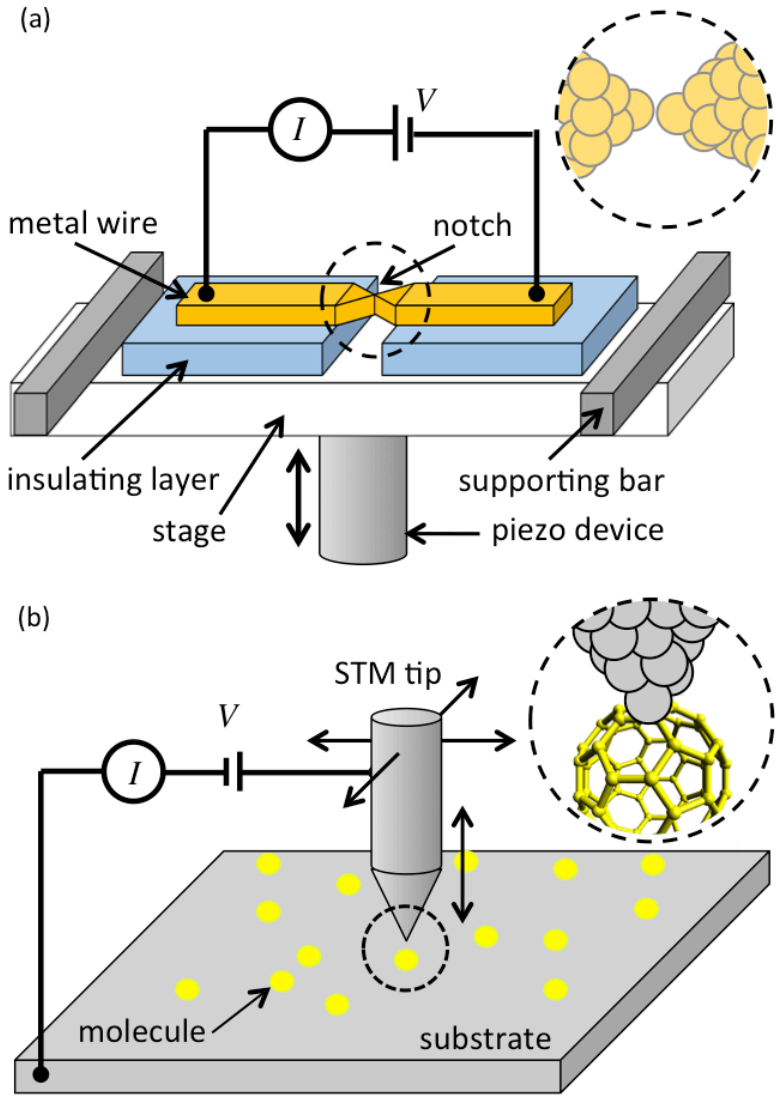

Fig. 3 Schematic illustrations of (a) mechanically controllable break junction (MCBJ) and (b) scanning tunneling microscopy (STM) junction. In MCBJ, a metallic wire with a notch is fixed on a stage. A piezoelectric device under the stage pushes and bends the stage so that the wire is broken and two electrodes are formed. The distance between the electrodes is controllable by adjusting the bend of the stage. In the STM junction, an STM tip is fixed over a molecule and is vertically moved until the tip contacts with the molecule.

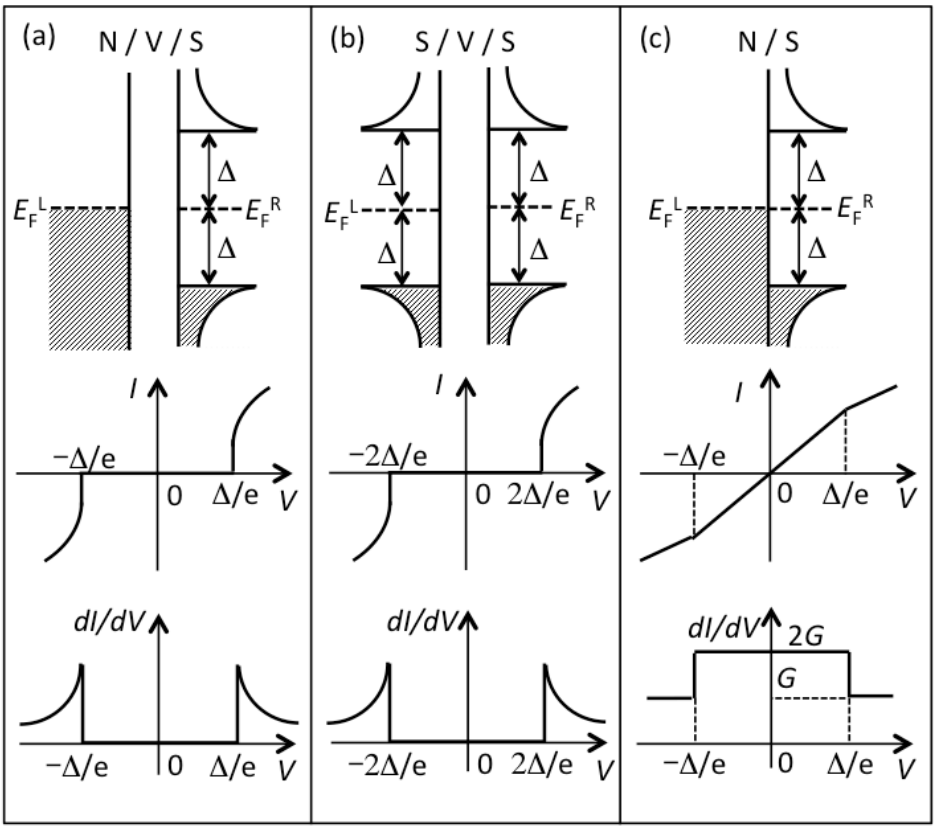

Fig. 4 Electronic structures, *I*-*V* and d*I*/d*V* spectra of (a) N/V/S, (b) S/V/S and (c) N/S junctions. N, V and S represent normal conductor, vacuum and superconductor, respectively.

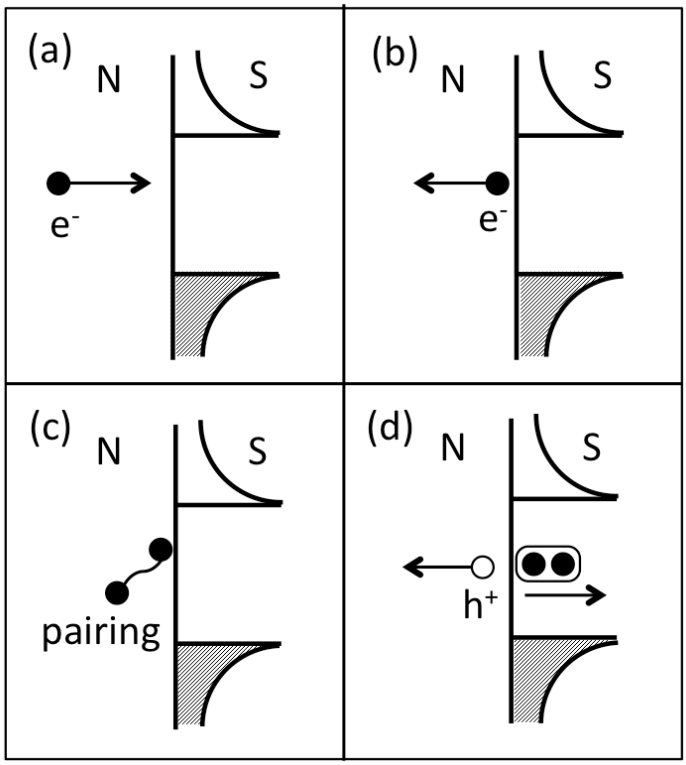

Fig. 5 Quasi-classical view of the Andreev reflection. (a) An electron from the left side normal conductor is incident to the N/S interface. (b) An electron is reflected by the superconducting gap. (c) and (d) An incident electron makes a Cooper pair with another electron at the interface to enter into the superconductor, and a hole formed simultaneously is reflected to the normal conductor. N and S represent normal conductor and superconductor, respectively.

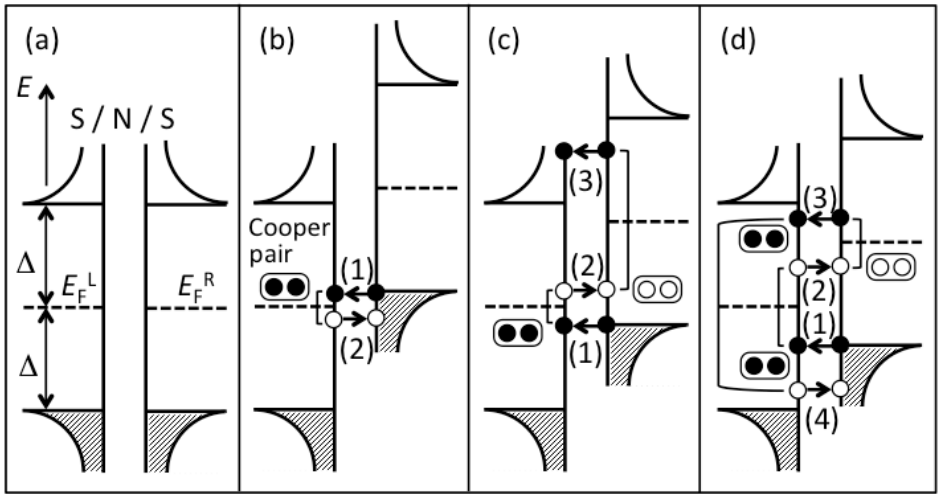

Fig. 6 Quasi-classical picture of multiple Andreev reflections. (a) Electronic structure of S/N/S junction. (b) Transport path via a single Andreev reflection at the bias voltage of $2\Delta/2 < eV < 2\Delta/1$. (c) Two-fold and (d) three-fold Andreev reflection processes occurring at the bias voltages of $2\Delta/3 < eV < 2\Delta/2$ and $2\Delta/4 < eV < 2\Delta/3$, respectively. N and S represent normal conductor and superconductor, respectively.

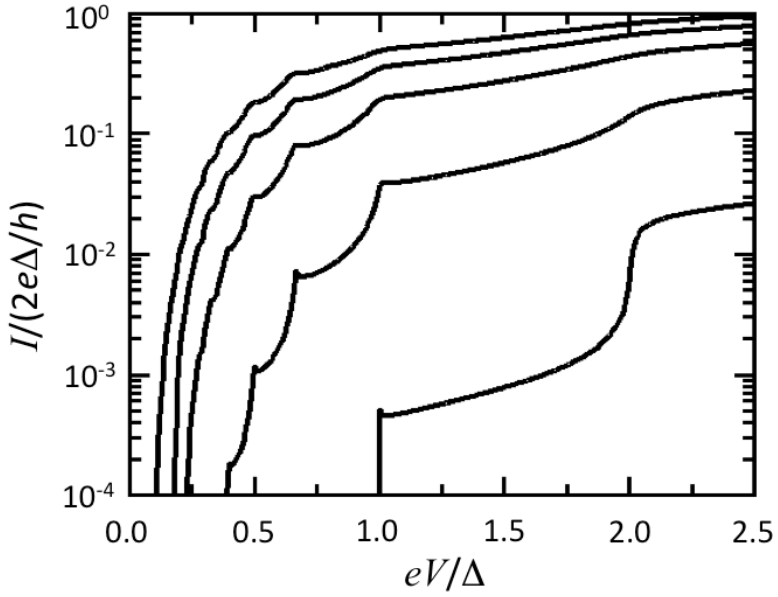

Fig. 7 *I-V* characteristics calculated for S/N/S junction of a single transport channel. Each *I-V* curve is calculated with the eq. (9) for τ = 0.7, 0.4, 0.3, 0.1 and 0.01 from the top to the bottom. The vertical axis is in the logarithmic scale. The stepwise increases of current in the voltage range of $V < 2\Delta/e$ originate from the MARs. This feature is in clear contrast with the *I-V* curve of the S/V/S junction shown in Fig. 4 (b).

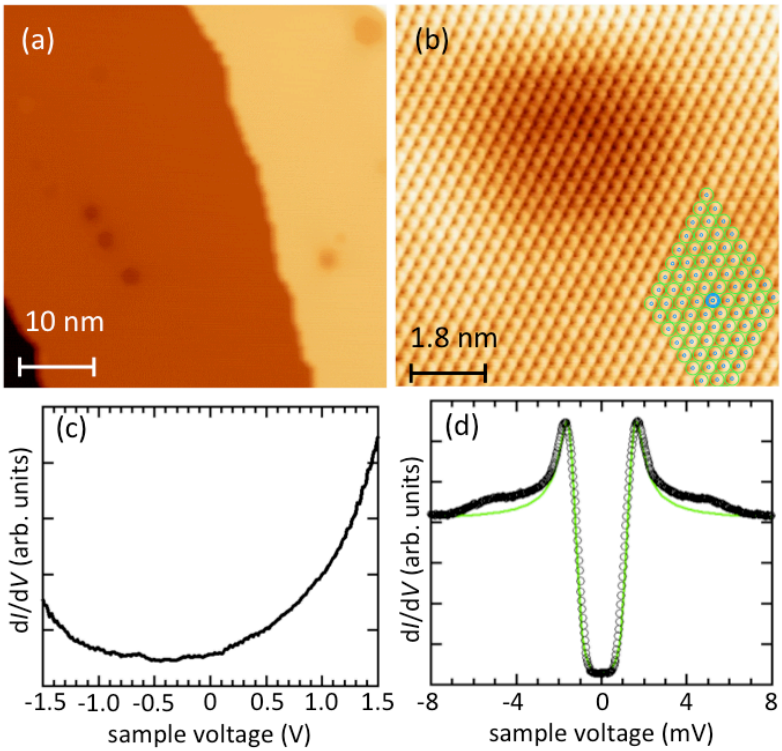

Fig. 8 STM topographic images of Pb(111) taken at (a) I_t = 100 pA and V_S = -100 mV (the image size is 50 x 50 nm^2) and (b) I_t = 1 μA and V_S = 50 mV (the image size is 9 x 9 nm^2). (c) and (d) show the STS spectra of Pb(111). The spectra were taken by fixing a tip over a terrace of Pb(111) with the feedback loop open (c) at 6 K with a modulation voltage of V_{rms} = 12 mV for the lock-in technique and (d) at 0.4 K with V_{rms} = 0.04 mV. The spectrum calculated with the Dynes function is also shown in (d).

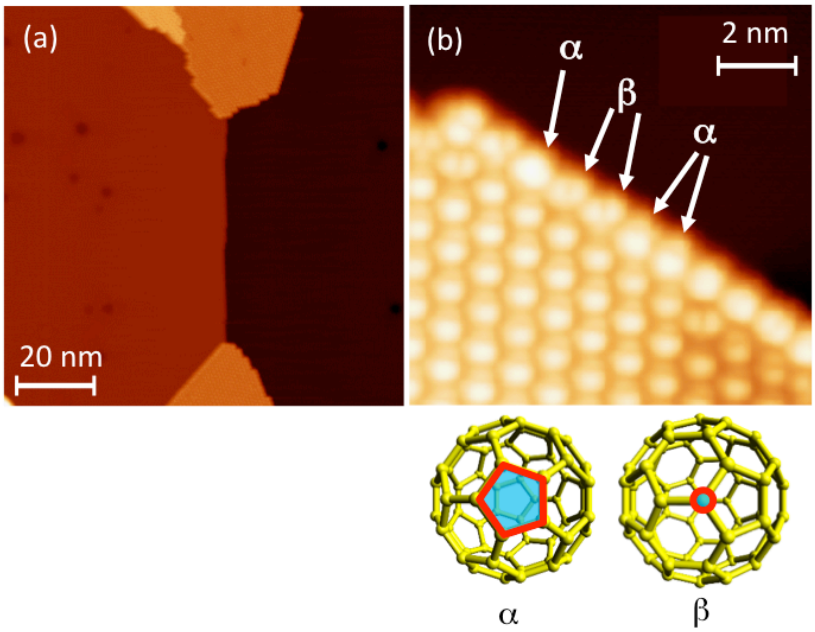

Fig. 9 STM topographic images of Pb(111) covered with C_{60} molecules taken at 0.4 K with (a) I_t = 50 pA and V_S = 1.0 V (the image size is 100 x 100 nm^2) and (b) I_t = 100 pA and V_S = -50 mV (the image size is 10 x 10 nm^2). Two types of C_{60} molecules (α and β) are observed in (b) as marked by arrows. The top views of α- and β-type molecules are also shown schematically in which the substrate atoms are omitted. In the contact measurement with STM, an STM tip approaches and touches a red pentagon (α-type molecule) and a small red circle (β-type molecule).

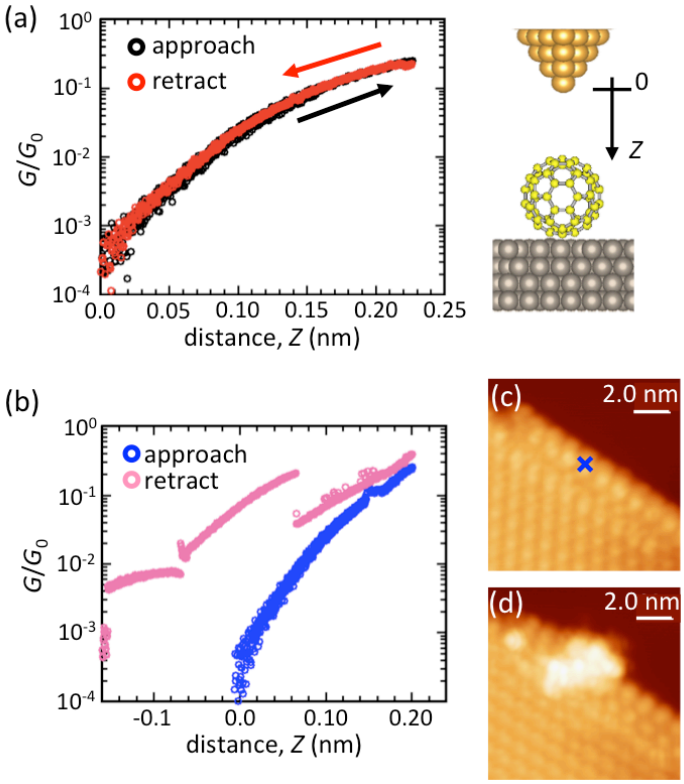

Fig. 10 Conductance traces as a function of distance of the tip (Z) (a) when the C_{60}-SMJ was successfully fabricated and (b) when the tip crashed into the sample surface. STM topographic images taken (c) before and (d) after measuring the trace in (b). Blue cross shows the target molecule. Irregular fluctuation of the conductance trace in (b) indicates that an atomic wire formed by the crash of the tip into the sample surface is partially broken in the uncontrollable manner.

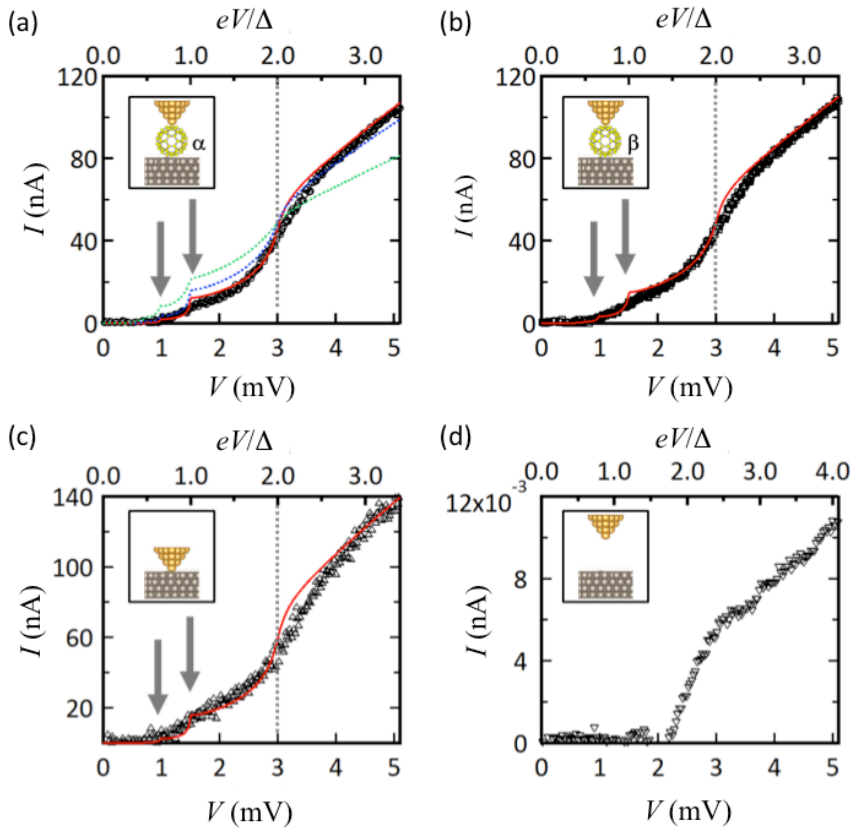

Fig.11 *I-V* characteristics measured at 0.4 K for (a) α-type C_{60}-SMJ, (b) β-type C_{60}-SMJ, (c) an atomic-sized contact formed by touching the Nb tip directly with the Pb substrate and (d) a vacuum junction consisting of the Nb tip, vacuum and the Pb substrate. The insets demonstrate the geometrical models of the junctions. The arrows mark the SGSs derived from the MARs. The dotted lines in (a) to (c) represent the border separating the inside and outside of the superconducting gap. The red curves in (a) to (c) are the best-fit results calculated with the eqs. (9) and (10) (see text). Green and blue curves in (a) show the calculated ones with n = 1 and n = 2, respectively.

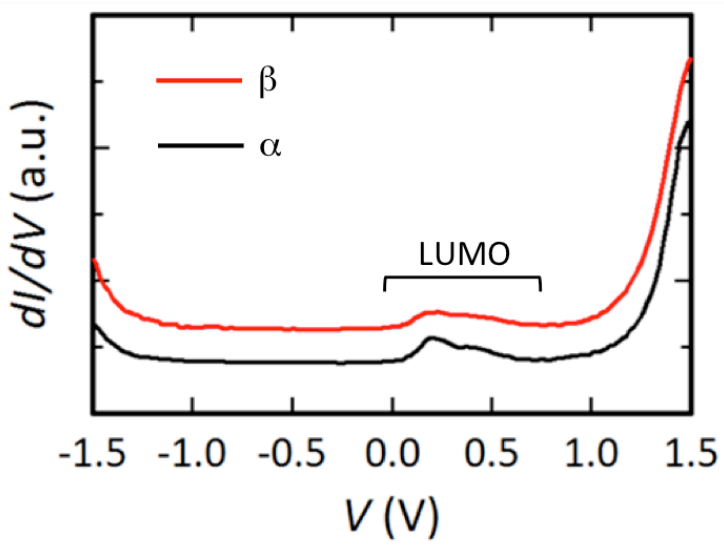

Fig. 12 STS spectra of the α- and β-type C_{60} molecules on Pb(111). The spectra were taken at 2.7 K by fixing the STM tip over the molecules with the feedback loop open and by adding a sinusoidal modulation voltage of V_{rms} = 16 mV to the sample voltage for lock-in measurement. The spectrum of β-type C_{60} molecule is vertically offset for clarity.